ACS CHEMICAL HEALTH & SAFETY

pubs.acs.org/acschas Article

Acetaminophen Sorption Using Invasive *Lantana camara* Biochar toward Achieving Sustainable Development Goals

Jonathan S. Singsit, Abhishek Kumar Chaubey, Manvendra Patel, and Dinesh Mohan*

Cite This: https://doi.org/10.1021/acs.chas.4c00036 Read Online

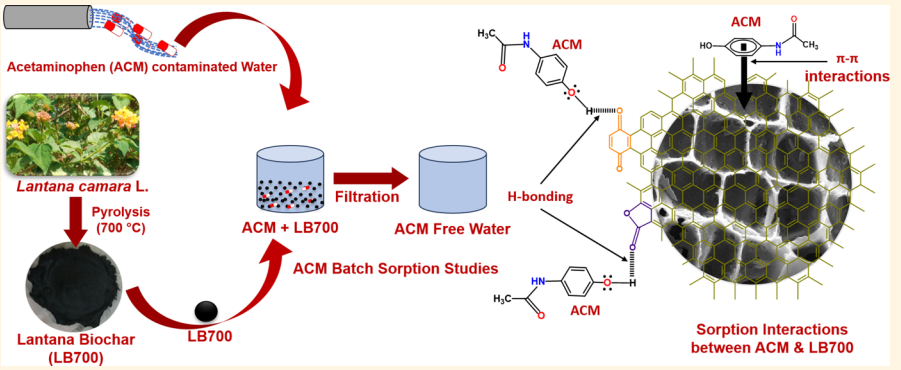

ABSTRACT: *Lantana camara* L., or simply *Lantana*, a widespread weed, was chosen to develop an eco-friendly biochar. *Lantana* contains toxic compounds such as triterpenoids and alkaloids, which can cause skin irritation and allergic reactions. Ingesting *Lantana* leaves can lead to severe symptoms, including nausea and liver damage. *Lantana* pollen can exacerbate respiratory conditions like asthma. Effective management strategies are essential to mitigate these health risks. Pharmaceutical pollution is an emerging crisis in wastewater and even groundwater. This is exacerbated by the huge global consumption of pharmaceuticals. Converting *Lantana* into biochar offers a solution that was tested for removing acetaminophen (ACM) as a model pharmaceutical compound, addressing both environmental and health concerns. *Lantana* is globally ranked among the top 10 worst invasive species. In India, ∼132,000 km^2 of pasture lands and ∼303,607 km^2 of forest lands are colonized by *Lantana*, making it a reliable biochar feedstock. *Lantana* biochar (LB700) was produced through slow pyrolysis of dried *Lantana* at 700 °C (ramp rate = 7 °C/min) and subsequently employed for aqueous ACM sorption. LB700 was characterized by its Brunauer−Emmett−Teller (BET) surface area, morphology, functional groups, crystallinity, and elemental composition. Batch ACM sorption was performed to find the influence of pH, initial ACM concentration, LB700 dose, and temperature. Equilibrium sorption data were interpreted using Freundlich, Langmuir, Temkin, Toth, Redlich−Peterson, and Sips isotherm models, while kinetic data were analyzed using pseudo-first- and second-order rate equations. Maximum ACM adsorption (4.5 mg/g) occurred at pH 2 with 1.0 g/L of LB700 dose. ACM sorption drastically reduced after pH 8 due to electrostatic repulsion between deprotonated ACM and negatively charged LB700. Pseudo-second-order equation best-fitted with kinetic data (R^2 = 0.91−0.97). A maximum Langmuir adsorption capacity of 13.2 mg/g was obtained at 40 °C. The spontaneity and endothermicity of the reaction were inferred from negative $\Delta G°$ (−19.73 to −24 kJ/mol) and positive $\Delta H°$ (20.82 kJ/mol) values, respectively. The $\pi-\pi$ stacking, H-bonding, van der Waals interactions, and pore diffusions are the dominant interactions. This study ingeniously addresses two pressing issues, *Lantana* invasion and pharmaceutical wastewater management, by providing an alternative solution through large-scale conversion of *Lantana* into biochar for treating pharmaceutical wastewater. Moreover, by converting *Lantana* into biochar, it effectively mitigates the health effects associated with this invasive plant, ensuring the preservation of environmental health and safety. Furthermore, it emphasizes the paramount importance for pharmaceutical industries to proactively treat their effluents, thereby safeguarding both environmental health and safety. Thus, this work strongly aligns with the United Nations Sustainable Development Goals including Clean Water and Sanitation (Goal 6) and Good Health and Well-Being (Goal 3).

continued...

Received: April 25, 2024
Revised: July 31, 2024
Accepted: September 4, 2024

KEYWORDS: *pharmaceutical, adsorption, biochar, invasive plants, health effects*

1. INTRODUCTION

The detection of pharmaceutical compounds in sewage treatment plants dates back to 1977.[1] Its occurrence in ground, surface, and drinking water sources is already established.[2−4] Globally, ∼631 pharmaceuticals were reported from 71 countries.[4] These "pseudo-persistent"[5] contaminants can bioaccumulate,[6] conduce antibiotic resistance, and alter soil microbiodiversity.[7] The increasing consumption of analgesics, antibiotics, and substances due to COVID-19 pandemic is worrisome.[8,9] These concerns behoove the need to find sustainable solutions to upgrade existing water treatment technologies to remove emerging contaminants in a cost-effective manner.[2,10−12]

Adsorption is widely used in treating industrial effluents and in drinking water treatment plants.[13−16] Powdered (PAC) and granular activated carbons (GAC)[16,17] and graphene[18,19] were applied for aqueous pharmaceutical removal. However, the high preparation costs of these materials retard its implementation as an adsorbent for water treatment in lower-income countries. Therefore, it is imperative to develop low-cost adsorbents using locally available feedstocks.[14,20]

Biochars were used in remediating aqueous organic[21−23] and inorganic contaminants,[24−27] including pharmaceuticals,[2,22,28−31,48,50] dyes,[32,33,51,52] endocrine disruptors,[34,35] volatile organic compounds,[36,37] pesticides,[21] heavy metals,[24,25,38,39,53,54] arsenic,[40,41,55−57] ammonia,[42,43] fluoride,[26] nitrate,[44,45] phosphate,[44] and other contaminants.[14,20,46−49]

In this study, *Lantana camara* L. biochar is prepared for aqueous acetaminophen removal. *Lantana* is an invasive plant with a marked presence in 75 countries.[58] Approximately 44% of 303,607 sq. km area of Indian forests is affected by *Lantana*.[58] *Lantana* is a threat to the forest biodiversity and livelihood of those dependent on forest produce.[58] Thus, *L. camara* L., a pervasive weed, was chosen to develop sustainable biochar. The plant contains toxic secondary metabolites including triterpenoids,[59,60] flavonoids,[61] and alkaloids,[61] which can cause dermatitis, hepatitis, jaundice, and photosensitivity upon ingestion.[59] Ingestion of *Lantana* leaves and berries, particularly by children or pets, can lead to nausea, vomiting, and diarrhea.[62] *Lantana* pollen can worsen existing respiratory conditions like allergic rhinitis and asthma in sensitive individuals.[63] Accordingly, it is vital to apply effective management and control strategies to reduce the health risks associated with *L. camara* L. Thus, *Lantana* was converted into biochar and then tested for its efficacy in safely removing a model pharmaceutical, acetaminophen. With a net primary productivity of ∼10−28 tons per hectare per year (t/ha/year) in subtropical and temperate forests, *Lantana* is presented as a suitable material for biochar production.[64] *Lantana*-derived biochar has been used for aqueous tartrazine[65] and chromium[54] removal. Acetaminophen, on the other hand, is an over-the-counter drug, making it easily accessible and widely consumed. Its presence in aquatic sources is reported in surface waters of >29 countries.[4,66] Sewage water concentrations of acetaminophen in Korea, China, United States, United Kingdom, and France ranged between 0.1 and 300 μg/L. It has also emerged as the most detected pharmaceutical in sewage waters from Taiwan and China.[66] Acetaminophen is also detected in wastewaters and surface water bodies in India with concentrations ranging between 4.5 and 86.8 μg/L.[67]

The current study proceeds with the development, characterization, and application of *Lantana* biochar for aqueous acetaminophen removal. Prepared biochar is characterized to evaluate its surface morphology, mineral phases, functional groups, and various physicochemical properties. Batch acetaminophen adsorption experiments were performed to evaluate the pH role, biochar concentration, initial acetaminophen concentration, and sorption temperature. Equilibrium sorption data were fitted to Freundlich, Langmuir, Temkin, Toth, Redlich−Peterson, and Sips isotherm equations, while kinetic data were fitted to pseudo-first- and second-order rate equations. Based on the experimental results, possible sorption interactions were also proposed.

Thus, conversion of *Lantana* into biochar not only offers a sustainable solution to combat the health effects linked with this invasive plant but also ensures the preservation of environmental health and safety. Additionally, this highlights the importance for pharmaceutical industries to treat their wastewater carefully, protecting environmental health and safety. These efforts strongly align with Sustainable Development Goal 6: Clean Water and Sanitation and Goal 3: Good Health and Well-being,[68] reflecting a holistic commitment to addressing pressing global challenges.

2. BIOCHAR DEVELOPMENT AND EXPERIMENTAL METHODOLOGIES

Analytical reagent (AR) and guaranteed reagent (GR) grades were used in this study. Acetaminophen ($C_8H_9NO_2$) (ACM) (structure given below) was purchased from Sigma-Aldrich.

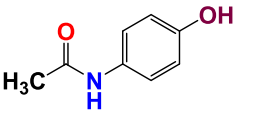

Acetaminophen (ACM) Structure

HCl and NaOH used to adjust the pH were procured from Merck and Qualigens, India, respectively. A Mettler Toledo, model AB 265-S/FACT instrument, was used to measure the weights of biochar and chemicals.

2.1. Biochar Preparation. *L. camara* L. woody biomass was collected from the Jawaharlal Nehru University campus, New Delhi (28.5402°N, 77.1662°E), India. Branches and twigs were chopped into small chips (2−3 cm in length), sun-dried, and subsequently dried in an oven (Scientech Instruments, India). The dried chips were transferred into a quartz crucible for slow pyrolysis at 700 °C in a muffle furnace (Thermolyne, model F6020C) at a heating ramp rate of 7 °C/min and a residence time of 30 min. The ramp rate of 7 °C/min was selected based on preliminary experiments. Furthermore, in the literature, ramp rates between 5 and 10 °C/min are commonly used for biochar preparation. The resulting *Lantana* biochar was ground and sieved into different particle size fractions. The biochar with a particle size of 50−100 B.S.S. mesh was washed with double distilled water to get rid of soluble organic residues and ash. The washed *Lantana* biochar (labeled as LB700) was oven-dried (at 60 °C for 48 h) and stored for further use in sorption studies.

https://doi.org/10.1021/acs.chas.4c00036
ACS Chem. Health Saf. XXXX, XXX, XXX−XXX

2.2. Lantana Biochar (LB700) Characterization. *2.2.1. pH_{pzc}.* The point of zero charge was determined using pH drift method.[31] 0.1 g of LB700 was mixed with 10 mL of 0.01 M NaCl solutions at pH values 2, 4, 6, 8, and 10. This suspension was agitated for 48 h at room temperature, and the final pH was measured. The pH_{pzc} was evaluated by plotting the initial pH against equilibrium pH.

2.2.2. Proximate and Ultimate Analysis. Ash content in biochar was determined as per ASTM D1762-84.[69] In brief, ash content was measured by combusting 0.5 g of LB700 in a quartz crucible (without lid) at 750 °C for 6 h in a furnace. CHNS analysis was carried out using a Thermo Finnigan Model FLASH EA 1112 series. The oxygen content of the biochar was estimated by subtraction. The LB700 surface area was determined by the Brunauer−Emmett−Teller (BET) method using a Micromeritics ASAP 2020 (accelerated surface area and porosimetry system) porosimeter employing nitrogen adsorption−desorption isotherms.

2.2.3. Morphology. Scanning electron microscopy (SEM) and transmission electron microscopy (TEM) were employed to examine the LB700 surface morphology. Biochar samples, affixed to a stainless steel stub using double-sided carbon tape, were analyzed using a Zeiss EVO 40 SEM at an acceleration voltage of 20 kV. A JEOL 2100F TEM set at 200 kV was used for high-resolution morphological images of biochar. Biochar samples were sonicated in ethanol for 15 min and loaded onto copper grids for TEM analysis.

2.2.4. Elemental and Spectral Identification. Energy-dispersive X-ray fluorescence (ED-XRF) spectrometry (PANalytical, model Epsilon 5) was used to estimate the bulk elemental composition of both pristine and loaded biochars. The biochar sample was pelleted through a hydraulic press after binding with polyvinyl acetate. An X-ray diffractometer (XRD) (PANalytical, model X'pert PRO) was used to determine the crystalline and mineralogical properties of the biochar. For XRD, the biochar sample was analyzed from 10 to 80° with a scan speed of 2°/min. Functional groups on pristine and ACM-loaded biochars were determined using attenuated total reflection-Fourier transform infrared spectrophotometer (ATR-FTIR) (PerkinElmer, model Frontier) in the range of 4000−650 cm^{-1} at a scan rate of 16 scans per second.

2.3. Sorption Studies. Solution pH, LB700 dose, contact time, ACM concentration, and temperature were optimized through batch sorption studies. These studies were performed at pH values of 2, 4, 5, 6, 8, and 10 (initial ACM conc. = 10 mg/L, LB700 dose = 1.0 g/L at 25 °C). The required pH value was adjusted using 0.1 N HCl and NaOH. LB700-ACM suspension was agitated for 24 h in a water bath shaker (Scientech and Macro Scientific Works, India). The suspension was then filtered using Whatman no. 1 filter paper. The filtrate was analyzed using a UV−Vis spectrophotometer at 243 nm (PerkinElmer, model Lambda 35). The equilibrium adsorption capacity is calculated using eq 1

$$q_e = \frac{(C_o - C_e)}{m} \times V \tag{1}$$

where q_e is the ACM amount adsorbed per gram of LB700 (mg/g); C_o and C_e are the initial and equilibrium ACM concentrations (mg/L), respectively; m is the amount of LB700 in grams; and V is the ACM volume (L) used in the batch sorption studies.

Kinetic studies, spanning from 5 min to 48 h, were conducted at different LB700 dosages (0.5, 1.0, and 2.0 g/L) with a fixed ACM concentration of 10 mg/L and at 25 °C. Sorption equilibrium studies were conducted with aqueous ACM concentrations ranging from 0.5 to 150 mg/L at a 1.0 g/L LB700 dose and at 10, 25, and 40 °C. All sorption studies were performed in triplicate, and the average values were reported.

2.4. Adsorption Modeling. Kinetic equations provide useful insights into reaction pathways and possible sorption interactions.[15,73] Thus, pseudo-first-order (PFO) rate equation[71] and pseudo-second-order (PSO) rate equation[72] were used to fit the kinetic data. Sorption isotherms describe the relationship (retention and mobility) between the liquid phase (adsorbate) and the solid phase (adsorbent) at a constant temperature and pH.[73] Langmuir,[74] Freundlich,[75] Temkin,[76] Redlich−Peterson,[77] Toth,[78] and Sips[79] isotherm models were used to fit the data and to better understand the sorption processes. Details about kinetic and isotherm equations are provided in Supporting Information, Section S1. Nonlinear kinetic and equilibrium isotherm model fitting was performed using Origin Pro 2018.

2.4.1. Thermodynamic Parameters. The spontaneity and nature of acetaminophen sorption onto LB700 were examined by calculating Gibbs free-energy change ($\Delta G°$), enthalpy change ($\Delta H°$), and entropy change ($\Delta S°$). $\Delta G°$, $\Delta H°$, and $\Delta S°$ were calculated using eqs 2 and 3

$$\Delta G^{\circ} = -RT \ln K_L \tag{2}$$

$$\ln K_L = -\frac{\Delta H^{\circ}}{R} \times \frac{1}{T} + \frac{\Delta S^{\circ}}{R} \tag{3}$$

where R is the universal gas constant (8.314 J/(mol K)), T is the temperature in Kelvin, and K_L is the Langmuir constant. The entropy change ($\Delta S°$) and enthalpy change ($\Delta H°$) were obtained from the intercept and slope, respectively, of a plot between $\ln K_L$ and $1/T$. $\Delta G°$ is calculated from eq 2.[80]

3. RESULTS AND DISCUSSION

3.1. Material Characterization. *3.1.1. Proximate and Ultimate Analysis.* The physicochemical characteristics of the developed LB700 are summarized in Table 1. Carbon, hydrogen, and nitrogen contents of LB700 were 76.88, 1.94, and 3.23%, respectively (Table 1). Oxygen and ash contents of LB700 were 12.76 and 5.19%, respectively. The pH_{pzc} of LB700 was 8.8 (Table 1). The BET surface area and mean pore volume of LB700 were 16.54 m^2/g and 0.012 cm^3/g, respectively (Table 1).

Table 1. Physicochemical Parameters of *Lantana* Biochar (LB700)

parameter	LB700
carbon (%)	76.88
hydrogen (%)	1.94
nitrogen (%)	3.23
oxygen (%)	12.76
ash (%)	5.19
pH_{pzc}	8.8
BET surface area (m^2/g)	16.54
mean pore volume (cm^3/g)	0.012
H/C	0.30
O/C	0.12

https://doi.org/10.1021/acs.chas.4c00036
ACS Chem. Health Saf. XXXX, XXX, XXX−XXX

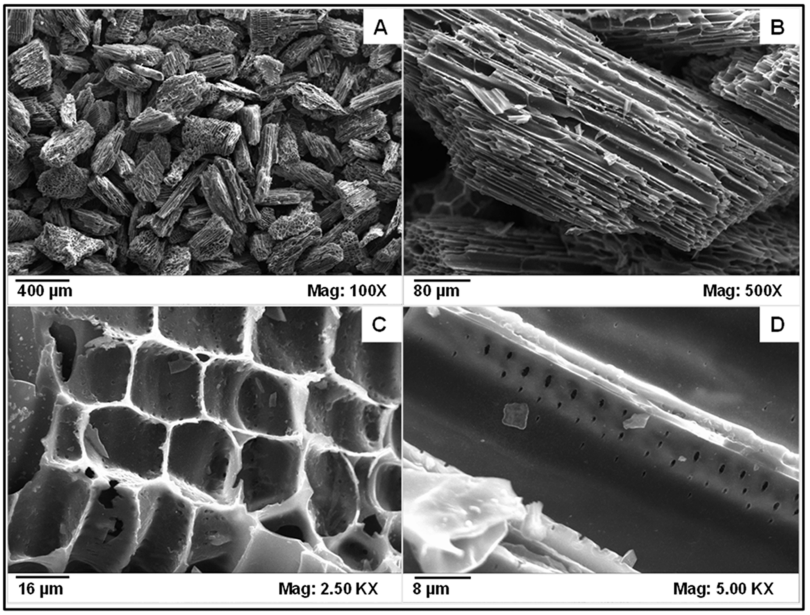

Figure 1. SEM micrographs of LB700 at (A) 100×, (B) 500×, (C) 2.5 KX, and (D) 5.0 KX.

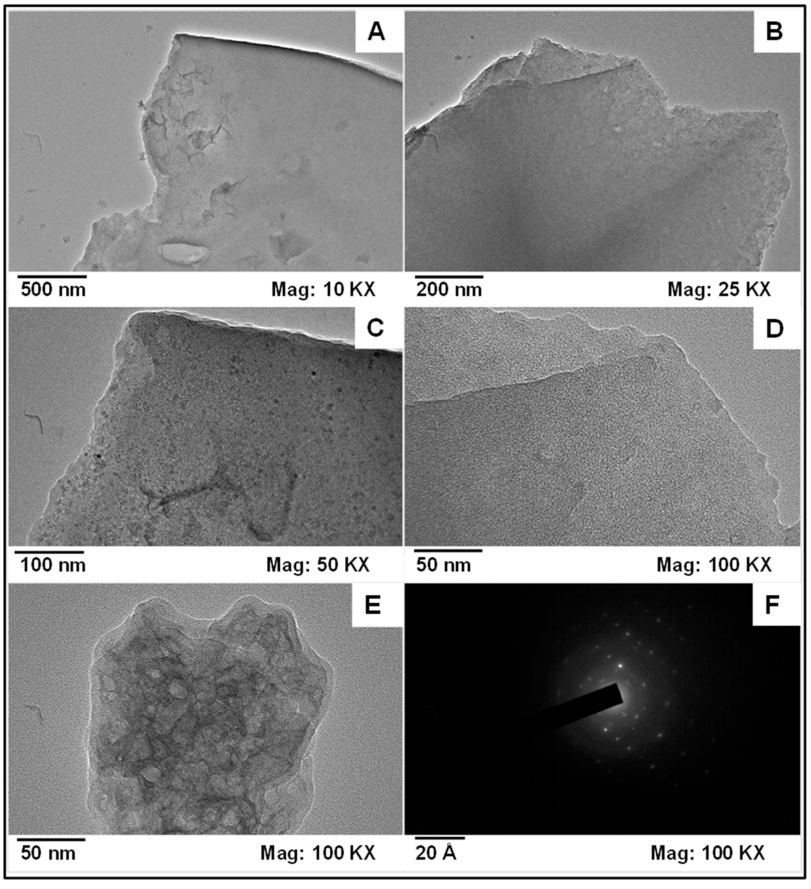

Figure 2. TEM micrographs of *Lantana* biochar at (A) 10 KX, (B) 25 KX, (C) 50 KX, (D) 100 KX, (E) 100 KX, and (F) SAED image.

LB700 had molar H/C and O/C ratios of 0.30 and 0.12, respectively. Biochar with H/C ratios <0.7 has more fused aromatic ring structures.[22,49,83,90] Biochar's stability is determined by its molar O/C ratio; a low ratio (<0.2) indicates stable carbon fraction.[22,49,83,90]

3.1.2. Surface Morphology of the LB700. The SEM images showed the pores of varying sizes (meso- and micropores) in LB700 (Figure 1). The plant structure is well preserved at 700 °C. In Figure 1, a carbonized skeleton of the internal plant structure is observed. Both superficial and internal porosities, visible as canal-like structures, are observed in LB700 (Figure 1). The low-magnification images (100x and 500X) show the intact or partially crumbled cell wall remnants of *Lantana* (Figure 1A,B). A high magnification (2.5 and 5.0 KX) shows

https://doi.org/10.1021/acs.chas.4c00036
ACS Chem. Health Saf. XXXX, XXX, XXX−XXX

the microporous nature of LB700 (Figure 1C,D). Pores with irregular shapes and sizes ranging from 16 to <2 μm are clearly visible (Figure 1C,D). Thus, LB700 exhibits a residual cellular structure with both meso- and microporosities.

TEM images and selected area electron diffraction (SAED) patterns of LB700 at different magnifications are shown in Figure 2. TEM images show the irregular shape edges and the presence of a layered structure in LB700 (Figure 2A−E). Dark spots in LB700 show a dense aromatic carbon aggregation (Figure 2C). The SAED pattern shows a nonuniform, disorderly diffraction pattern, suggesting the presence of polycrystalline structures occurring in different phases and orientations (Figure 2F).[81]

3.1.3. Elemental Composition of LB700. Elemental composition of LB700 was determined using ED-XRF analysis (Table 2). This indicates the potential role of these minerals in acetaminophen sorption.

Table 2. Elemental Composition of LB700 as Determined Using ED-XRF

elements	values
MgO (%)[a]	0.81
SiO_2 (%)[a]	0.41
P_2O_5 (%)[a]	0.89
SO_3 (%)[a]	0.56
K_2O (%)[a]	0.73
CaO (%)[a]	1.74
Fe_2O_3 (ppm)[a]	920.7
Cl (ppm)	127.2
W (ppm)	117.7
Sr (ppm)	114.6
Ti (ppm)	66.7
MnO (ppm)	86.2
Cu (ppm)	44.8
Zn (ppm)	74.6

[a](as oxides).

3.1.4. XRD Pattern of LB700. XRD pattern of LB700 shows two broad humps centered at 2θ = 24.73° (hkl = 002) and 43.64° (hkl = 100) (Figure 3). The peak at 2θ = 24.73° corresponds to the presence of amorphous carbon in biochar. However, the peak at 2θ = 43.64° is indicative of the formation of carbonized aromatic and condensed planes of turbostratic carbon in biochar.[82,83] A sharp peak at 26.35° and 72.58° reveals the presence of SiO_2 (quartz) in LB700.[83] Other sharp peaks at 29.25, 43.64, and 51.16° indicate the presence of $CaCO_3$ (calcites).[21,82] The abundances of calcite and silicate in the XRD spectrum of LB700 corroborate the elemental data (Table 2).

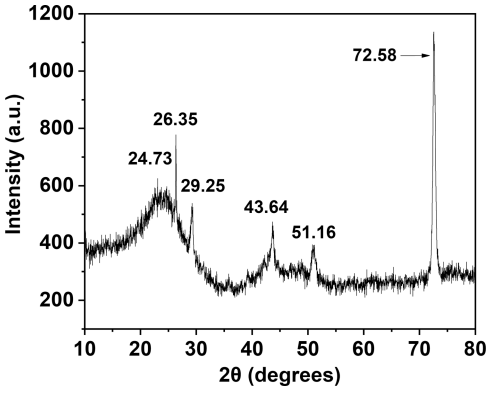

Figure 3. XRD pattern of *Lantana* biochar (LB700).

3.1.5. FTIR Spectra of Pristine and ACM-Loaded LB700. The FTIR spectra of pristine LB700 and ACM-loaded LB700 obtained between 650 and 4000 cm^{-1} are shown in Figure 4.

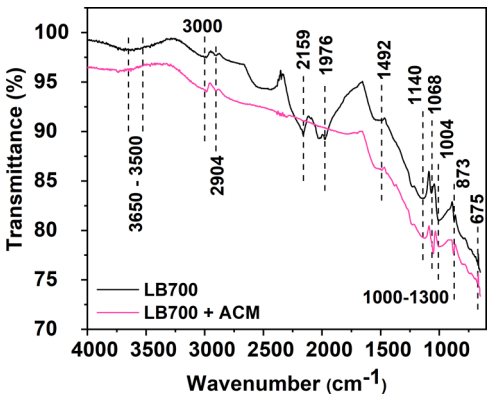

Figure 4. FTIR-ATR spectra of pristine and ACM-loaded *Lantana* biochar (LB700).

Identified peaks indicate the presence of oxygen-containing functional groups (C═O, C−O, and −OH) along with aliphatic and aromatic functional groups (C═C and C−H). Both pristine and ACM-loaded LB700 spectra show the −OH peaks at 3500−3650 cm^{-1}.[84] The strong peaks at 1068 and 1004 cm^{-1} indicate the presence of bonded hydroxyl groups.[84] The peak at 3000 cm^{-1} suggests the C−H stretching vibrations arising from aromatic, alkene, and alkyne groups.[84] A small peak at 2904 cm^{-1} shows the presence of asymmetric aliphatic CH_2 groups. The stretching of the ether group's carbon−oxygen bonds is detected at approximately 1492 cm^{-1}.[85] The C−O stretching in esters exhibits a distinctive peak within the range of 1000−1300 cm^{-1} (Figure 4). A peak around 1140 cm^{-1} indicates a phenyl acetate group. Alkene is deduced from C−H bending vibrations found around 873 cm^{-1} where polynuclear aromatic groups are known to have characteristic absorption between 675 and 900 cm^{-1}.[84] A reduction in the intensity of ACM-loaded biochar compared to that of pristine biochar indicates the participation of functional groups in the adsorption process.[24] The disappearance of symmetric and asymmetric C═O stretchings, observed at 2159 and 1976 cm^{-1} (lactone, quinone, or ester functional groups), is clearly evident in ACM-loaded LB700, highlighting their significant role in acetaminophen sorption.[85]

3.2. Batch Sorption Studies. *3.2.1. Initial pH Effect.* Solution pH plays an important role in ACM sorption by influencing the surface charge of LB700 and acetaminophen species. Acetaminophen removal was carried out over a pH range of 2−10 using LB700 (Figure 5). Acetaminophen (pK_a = 9.38) remains nonionized within the pH range of 2−8, while LB700 is positively charged (pH_{pzc} = 8.8). Maximum acetaminophen sorption was achieved at pH = 2. A rapid decline in acetaminophen sorption was recorded between pH 2 and 5, stabilizing thereafter until pH 8. After pH = 8, ACM sorption is drastically reduced (Figure 5). This reduction is attributed to electrostatic repulsion between deprotonated ACM and negatively charged LB700. A similar ACM sorption

https://doi.org/10.1021/acs.chas.4c00036
ACS Chem. Health Saf. XXXX, XXX, XXX−XXX

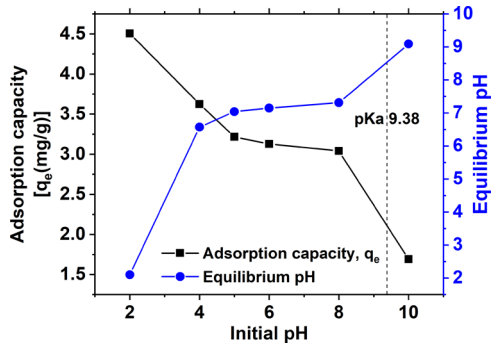

Figure 5. pH effect on acetaminophen sorption onto LB700.

pattern was previously reported.[22,28,52,86] In view of the above information, all sorption studies were performed at pH 5.

3.2.2. Acetaminophen Sorption Kinetics. Acetaminophen sorption kinetic studies were conducted using LB700 doses of 0.5, 1.0, and 2.0 g/L at a fixed 10 mg/L acetaminophen concentration. The contact time varied from 5 min to 48 h. An increase in the LB700 dose led to a corresponding increase in the percent ACM adsorption. At 2.0 g/L LB700 dose, ∼50% ACM removal was obtained within 2 h, which increased to >92% at an equilibrium after 24 h (Figure 6 and Figure S1). Overall, maximum ACM sorption of 92% was achieved at 2.0 g/L LB700 dose, which decreased to 84 and 62% at 1.0 and 0.5 g/L LB700 dosages, respectively (Table 3). Sorption kinetics data were fitted to nonlinear pseudo-first and pseudo-second-order rate eqs [Figure 6(A-B)]. Pseudo-second-order equation best-fitted with kinetic data at all of the LB700 dosages (R^2 = 0.913 at 0.5 g/L, 0.912 at 1.0 g/L and 0.968 at 2.0 g/L) (Table 3).

3.2.3. Acetaminophen Sorption Isotherm Studies. Sorption equilibrium studies were performed to determine the monolayer LB700 adsorption capacity across ACM concentrations ranging from 0.5 to 150 mg/L at 10, 25, and 40 °C with a fixed LB700 dose of 1.0 g/L. Sorption equilibrium data were fitted to nonlinear Freundlich, Langmuir, Temkin, Toth, Redlich−Peterson, and Sips isotherm equations [Figure 7(A-F)]. Langmuir, Redlich−Peterson, and Sips and Toth models best-fitted the equilibrium data with high correlation coefficients (R^2 > 0.95 at 25 and 40 °C) (Table 4). Langmuir sorption capacities of 9.8 (at 10 °C), 12.1 (at 25 °C), and 13.2 (at 40 °C) mg/g were obtained (Table 4). Langmuir sorption capacity increased with an increase in temperature, confirming the endothermic nature of acetaminophen sorption on LB700. It is inferred that due to high correlations of data with Langmuir, Sips, Toth, and Redlich−Peterson models, a simultaneous execution of homogeneous monolayer/multilayer and heterogeneous sorption takes place.[22] The decreasing Freundlich adsorption intensity values ($1/n$) indicate an increasing sorption heterogeneity with an increase in temperature (Table 4).[73] The Redlich−Peterson model incorporates certain aspects of both Langmuir and Freundlich models. Since the constants are <1, whereas g = 1, implying that Langmuir fitting is assumed.[73]

3.2.4. Thermodynamic Parameters. Thermodynamic parameters of the acetaminophen sorption on LB700 were evaluated and are presented in Table 5. The slope and intercept from Van't Hoff plots were used to estimate the change in enthalpy ($\Delta H°$) and entropy ($\Delta S°$), respectively. The positive $\Delta H°$ and $\Delta S°$ values showed the endothermic nature and increasing randomness of the sorption with an increase in temperature.[70,80] Negative $\Delta G°$ values indicate that sorption is spontaneous in nature and feasible.[21,80] Negative Gibbs free-energy ($\Delta G°$) values were previously reported for acetaminophen removal on Brazil nutshells[70] and olive stones activated carbon.[87]

3.2.5. Potential Sorption Interactions of Acetaminophen with L. camara Biochar. Acetaminophen sorption depends on solution pH, temperature, adsorbate pK_a, and adsorbent (*L. camara* biochar) characteristics including surface area, pore size distribution, and surface functional groups.[2,52,85−88]

The effect of the solution pH is explained in Section 3.2.1 (Figure 5). LB700 functional groups before and after acetaminophen sorption through FTIR spectroscopy provide useful insights (Figure 4). A complete loss of peaks at 2159 and 1976 cm^{-1} indicates the extensive involvement of carbonyl (C═O) functional groups in acetaminophen sorption. Possible acetaminophen sorption interactions are given in Figures 8(A-D) and 9(A-B).

Acetaminophen speciation is given in Figure 8A while its H-bonding with phenolic, lactone, and quinone groups in the biochar is shown in Figure 8(B,C). These H-bondings are facilitated by the presence of amide and hydroxyl groups in acetaminophen and the quinone and lactone groups present in the biochar. $\pi-\pi$ donor−acceptor interactions are observed between electron-deficient aromatic rings in the biochar and the electron-rich phenyl ring of acetaminophen (Figure 8D). Adsorption of acetaminophen by $\pi-\pi$ interactions and H-bonding with carbonaceous materials is known to be dominant

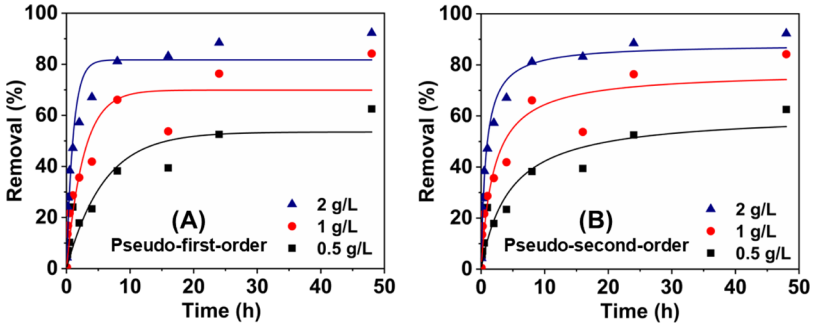

Figure 6. Acetaminophen rate sorption data fitted to (A) pseudo-first-order and (B) pseudo-second-order rate equations [pH = 5; LB700 particle size = 50−100 BSS mesh, ACM concentration = 10 mg/L; shaking speed = 100 rpm; temperature = 25 °C] at 0.5, 1.0, and 2.0 g/L LB700 dosages. Points represent the experimental data, while the solid lines show the fitting of nonlinear kinetic equations to the experimental data (Figure 6 shows only the percent removal kinetics).

https://doi.org/10.1021/acs.chas.4c00036
ACS Chem. Health Saf. XXXX, XXX, XXX−XXX

Table 3. Nonlinear Kinetic Equation Rate Constants Obtained at Different LB700 Dosages and Contact Times[a]

		Pseudo-first order rate constants			Pseudo-second order rate constant		
LB700 (g/L)	experimental ACM sorption capacity, mg/g (%)[b]	q_e, mg/g(%)[b]	k_1 (h^{-1})	R^2	q_e, mg/g(%)[b]	k_2 ($gmg^{-1}h^{-1}$)	R^2
0.5	12.08 (62)	10.34 (53)	0.17	0.871	11.80(61)	0.02	0.913
1.0	8.13 (84)	6.75 (70)	0.37	0.865	7.47 (78)	0.07	0.912
2.0	4.45 (92)	3.95 (82)	0.96	0.908	4.25 (90)	0.31	0.968

[a]pH = 5; LB700 particle size = 50−100 BSS mesh; acetaminophen concentration = 10 mg/L; shaking speed = 100 rpm; temperature = 25 °C. [b]Percent removal is given in parenthesis.

Table 4. Nonlinear Isotherm Parameters Obtained at Different Acetaminophen Concentrations and Temperatures[a]

	temperature (^{0}C)		
isotherm parameter	10	25	40
	Freundlich		
K_F (mg/g)	1.00	1.67	1.89
n	2.34	2.47	2.49
R^2	0.78	0.89	0.90
	Langmuir		
Q^0 (mg/g)	9.84	12.09	13.22
K_L (L/mg)	0.03	0.062	0.07
R^2	0.84	0.95	0.96
	Temkin		
b_T (kJ/mol)	1399	1080	1016
a_T (L/mg)	0.62	1.24	1.46
R^2	0.77	0.91	0.94
	Redlich−Peterson		
K_{RP} (L/g)	0.29	0.75	0.88
a_{RP} $(mg/L)^{-g}$	0.03	0.06	0.07
g	1.00	1.00	1.00
R^2	0.82	0.95	0.96
	Sips		
K_{LF} (L/g)	0.07	0.71	0.87
α_{LF} (L/mg)	0.01	0.06	0.07
β_S	1.50	1.03	1.01
R^2	0.85	0.95	0.96
	Toth		
K_T (mg/g)	1.61	2553	381
a_T (L/mg)	269.6	75.5	51.1
t	0.28	0.51	0.62
R^2	0.83	0.96	0.97

[a]pH = 5, LB700 dose = 1 g/L; LB700 particle size = 50−100 BSS mesh; equilibrium time = 24 h; shaking speed = 100 rpm.

sorption interactions.[22,28,29,89] The amides are weak electron donors to the phenyl ring, while −OH groups are strong electron donors to the phenyl ring. They both enrich the π−electron density on the acetaminophen ring, allowing it to be a π-donor.[86]

LB700 contains monovalent and divalent metal oxides (MgO, CaO, K_2O, Fe_2O_3, and SiO_2) (Table 2). These solvated metal ions can interact with acetaminophen (Figure 9A,B). The presence of C−O$^-$ and C═O groups on the biochar surface enables the formation of a char coordination with transition metal. This coordination complex in turn forms resonance hybrid structures with ionized acetaminophen (Figure 9A). Another possible interaction is through the formation of a metal π-complex with the electron-dense graphitic center of biochar (Figure 9B_i). The metal then binds with ionized acetaminophen, lowering its formal charge in the process (Figure 9B_{ii}).

Pore diffusion takes place during organic contaminant sorption onto carbonaceous adsorbents.[2,21,90] Mass transfer of solutes occurs around the surface of the adsorbent, following which pore diffusion takes the sorbate molecules into the pores. As the pores get smaller, the adsorbed molecules equilibrate by being trapped inside the porous network. The more the number of molecules entering the smaller pores, the likelier it is to get trapped [Figure 10(A-C)]. The presence of meso- and micropores play a significant role in acetaminophen diffusion into LB700 (Figure 10).

Biochar has previously been reported as a three-dimensional (3D) adsorbent, meaning that the presence of oxygen (10−20 wt %) in biochar induces a swelling behavior upon its immersion in aqueous media.[91] These biochars are usually prepared at lower temperatures and shorter pyrolysis times. Thus, they are likely to exhibit swelling in water in biochar regions with a higher oxygen content. This swelling enhances the overall acetaminophen sorption by opening up the isolated dry pores.[31] LB700 contains 12.76% oxygen. Regions with plentiful oxygen-containing groups are prone to swelling, which ensures that acetaminophen gets sorbed within this framework of the LB700. This phenomenon is evident when sorption capacities of different adsorbents with higher surface areas are compared (Table 6). A higher oxygen content LB700 (BET surface area = 16.54 m^2/g) gives an adsorption capacity of 0.799 mg/m^2, which is 3−10 times higher as compared to the adsorption capacities (0.074 and 0.221 mg/m^2) of various other adsorbents (Table 6).

Acetaminophen and LB700 have a wide range of favorable interactions, of which only a few important instances are provided here. Across a wide pH range and environmental matrix, the sorption mechanisms alter; thus, applying advanced techniques including molecular dynamic simulations such as density function theory (DFT) and Monte Carlo simulations are recommended for future studies. Similarly, the application of advanced spectroscopic techniques such as XPS and near-edge X-ray absorption spectroscopy (NEXAS) can be examined for in-depth molecular interaction insights in the future. Furthermore, LB700 can be used to remove many other pharmaceuticals from water.

4. CONCLUSIONS

Lantana biochar (LB700) was successfully prepared, characterized, and used for acetaminophen remediation. LB700 was characterized by its heterogeneous carbonaceous structure, featuring many meso- and micropores. All batch sorption equilibrium and kinetic studies were carried out at pH 5.0 and 1.0 g/L LB700 dose. Langmuir adsorption capacities of 9.84, 12.09, and 13.22 mg/g were obtained at 10, 25, and 40 °C, respectively. No single sorption model describes the acetaminophen sorption on LB700 due to its heterogeneous nature. At 25 and 40 °C, Langmuir, Sips, Redlich−Peterson, and Toth isotherm models (R^2 > 0.95) suggest the

https://doi.org/10.1021/acs.chas.4c00036
ACS Chem. Health Saf. XXXX, XXX, XXX−XXX

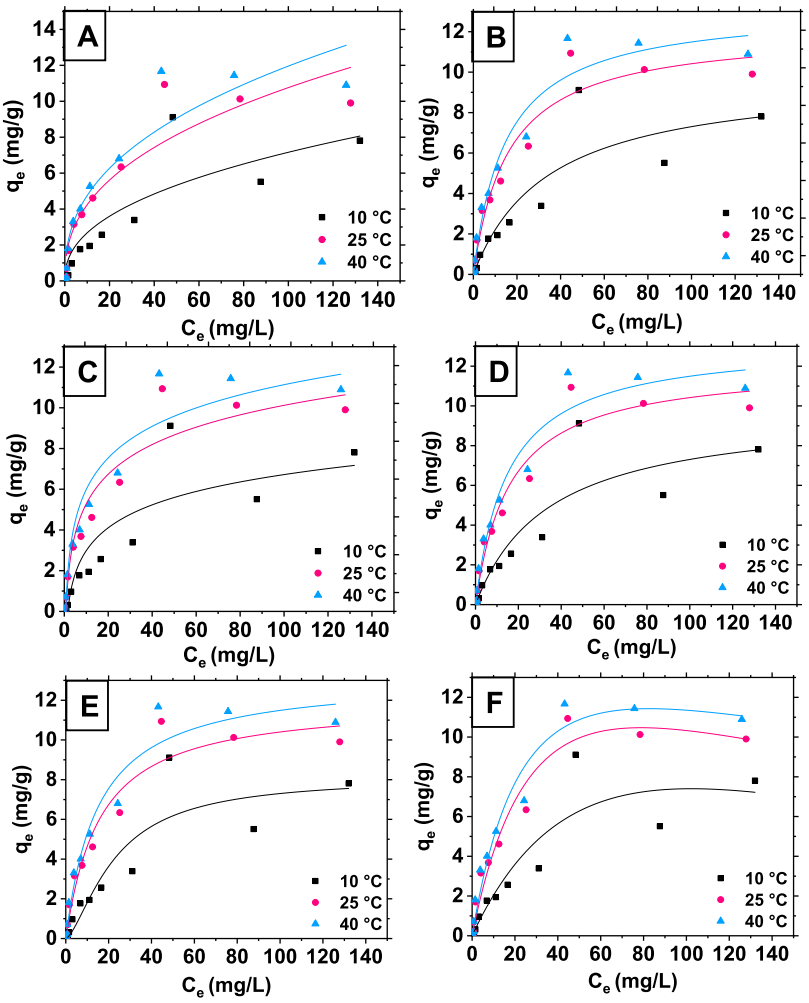

Figure 7. Acetaminophen sorption data fitted to (A) Freundlich, (B) Langmuir, (C) Temkin, (D) Redlich−Peterson, (E) Sips, and (F) Toth isotherm models [pH = 5, adsorbent (LB700) dose = 1 g/L; LB700 particle size = 50−100 BSS mesh; equilibrium time = 24 h; shaking speed = 100 rpm] at different acetaminophen concentrations (0.5−150 mg/L). Points represent the experimental data, and the solid lines show the isotherm model fitting to the experimental data.

Table 5. Thermodynamic Parameters for Acetaminophen Sorption on LB700[a]

$\Delta G°$(kJ/mol)				
10 °C	25 °C	40 °C	$\Delta H°$(kJ/mol)	$\Delta S°$ (kJ/mol·K)
−19.73	−22.67	−24.00	20.82	0.14

[a]pH = 5, adsorbent (LB700) dose = 1 g/L; particle size = 50−100 BSS mesh, acetaminophen concentration = 0.5−150 mg/L; equilibrium time = 24 h; shaking speed = 100 rpm at different temperatures.

involvement of simultaneous multiple interactions between acetaminophen and LB700. Oxygen-containing functional groups including carbonyl, lactone, and quinone provided useful interactions with acetaminophen through H-bonding. The aromatic carbon in the biochar enabled $\pi-\pi$ interactions along with pore filling. The presence of metal oxides gave rise to electrostatic interactions. Thermodynamic parameters revealed a spontaneous and endothermic nature of acetaminophen sorption on LB700.

The LB700 dosage of 1 g/L can effectively remove acetaminophen at pH 5.0 and 25−40 °C. Its adsorption capacity per surface area (mg/m^2) is better or comparable to many other biochars (Table 6). Thus, LB700 can effectively clean pharmaceutical-contaminated water at pH 5.8−7.8 and ∼20 °C. Future research could benefit from exploring additional modifications of LB700 by taking advantages of the dominating mechanisms mentioned above in order to enhance the adsorption of organic contaminants. Similarly, there are multiple region-specific invasive plants that can be examined using similar studies reported in this paper. Furthermore, biochar developed from *Lantana* can also be tested for different organic contaminants including pesticides and PFAS.

Our study demonstrates a commitment to addressing urgent global challenges by aligning with sustainable development goals (SDGs) viz., SDG-6: Clean Water and Sanitation and SDG-3: Good Health and Well-Being. Rethinking wastewater treatment with innovative measures ensures the active preservation of environmental health and safety. *L. camara* L. was successfully evaluated for aqueous acetaminophen remediation. Thus, converting *Lantana* into biochar offers a sustainable solution to deal with emerging contaminants in water, simultaneously combating the health effects of this invasive plant and mitigating its adverse effects on the environment. Thus, the use of an invasive plant that threatens

https://doi.org/10.1021/acs.chas.4c00036
ACS Chem. Health Saf. XXXX, XXX, XXX−XXX

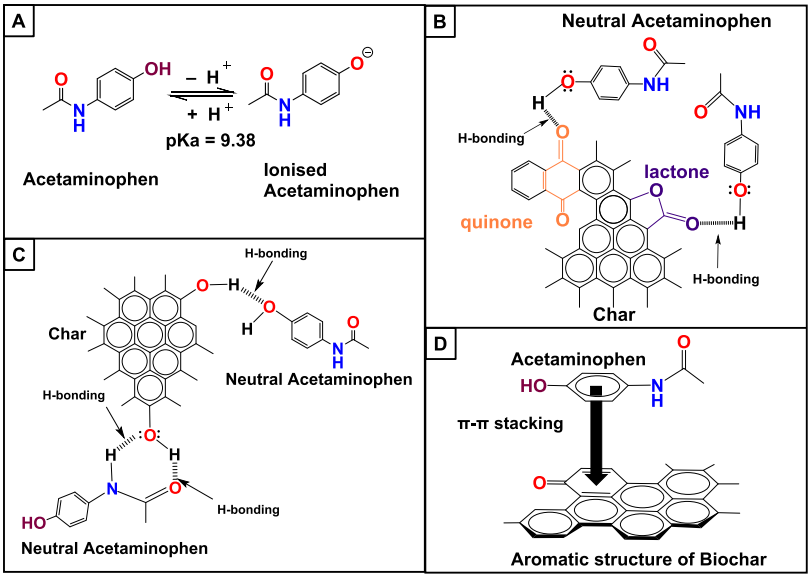

Figure 8. Potential acetaminophen sorption interactions: (A) acetaminophen speciation, (B) H-bonding to biochar's quinone and lactone groups, (C) surface H-bonding with phenolic groups of biochar, and (D) $\pi-\pi$ interactions between biochar and acetaminophen (H-bonding indicated by arrows → in B and C).

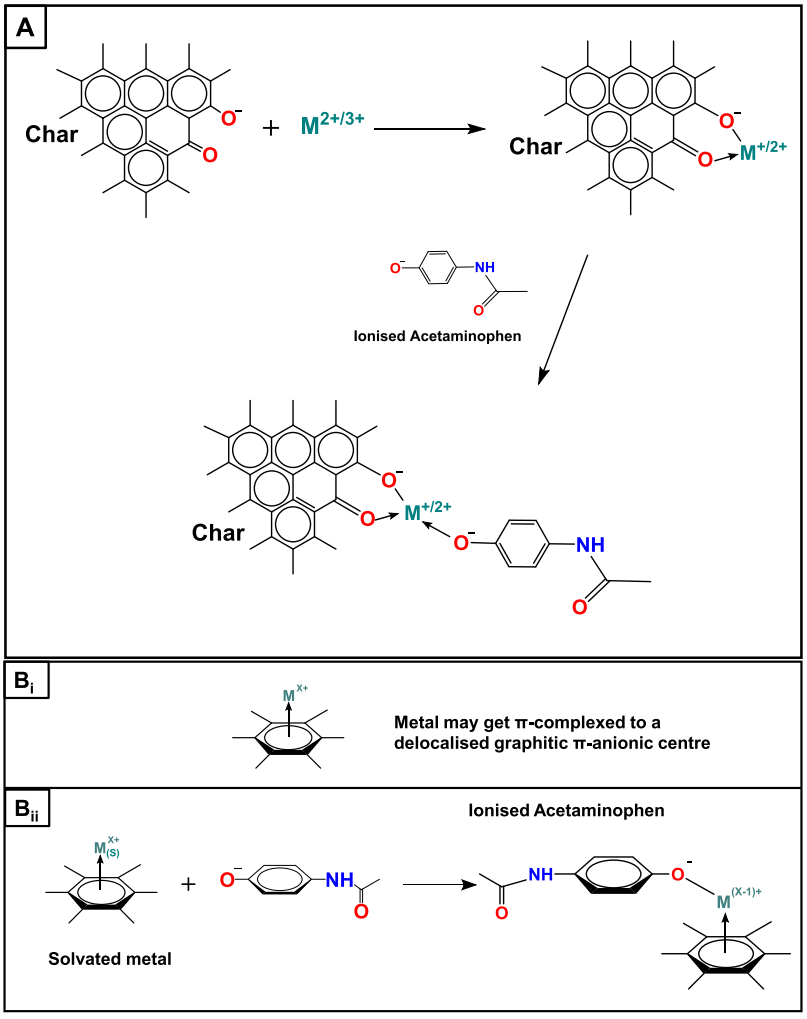

Figure 9. (A) Solvated transition metal ($M^{2+/3+}$) coordinates with char and forms a resonance hybrid structure with acetaminophen. (B_i) Transition-metal-forming π-complex with π-anionic center of graphitic carbon, (B_{ii}) bonding of metal with ionized acetaminophen.

https://doi.org/10.1021/acs.chas.4c00036
ACS Chem. Health Saf. XXXX, XXX, XXX−XXX

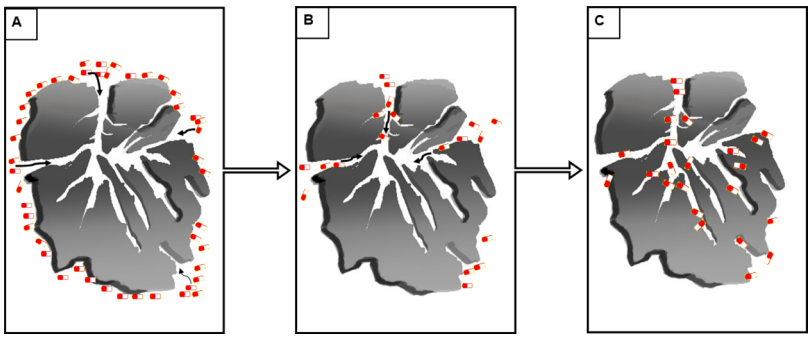

Figure 10. (A) ACM adsorption on LB700 surface; (B) pore diffusion of ACM; and (C) ACM trapping in the porous network of LB700.

Table 6. Comparative Acetaminophen Adsorption Capacities (in mg/g and mg/m^2) of Lantana Biochar (LB700) and Other High Surface Area Adsorbents

adsorbent	pH	temp. (°C)	surface area (m^2/g)	adsorption capacity (mg/g)	adsorption capacity per surface area (mg/m^2)	references
banana peel biochar	3	25	587.47	49.43	0.084	22
nonspherical biochar (glucose-derived)	7	10	1033	147	0.142	29
spherical biochar (glucose-derived)	7	10	1292	286	0.221	29
pulp mill sludge biochar	7.6	25	209.12	15.53	0.074	92
MgO/Al_2O_3 biochar	6	25	419	108.7	0.259	50
oak Acorn AC (KOH)	3	25	298	64.92	0.218	93
oak Acorn activated carbon (H_3PO_4)	3	25	234.6	46.87	0.2	93
Brazilian nutshells activated carbon 1.0 ($ZnCl_2$)	7	25	1457	284.6	0.195	70
Brazilian nutshells activated carbon 1.5 ($ZnCl_2$)	7	25	1640	309.3	0.189	70
Industrial pretreated cork activated carbon (steam)	5	30	750	118.6	0.158	94
commercial activated carbon	7	25	1248	221	0.177	95
LB700	**5**	**10**	**16.54**	**9.84**	**0.595**	**this study**
LB700	**5**	**25**	**16.54**	**12.09**	**0.731**	**this study**
LB700	**5**	**40**	**16.54**	**13.22**	**0.799**	**this study**

biodiversity and agricultural land offers an innovative approach towards two global crises.

■ ASSOCIATED CONTENT

Supporting Information

The Supporting Information is available free of charge at https://pubs.acs.org/doi/10.1021/acs.chas.4c00036.

Detailed information on the sorption kinetic equations, isotherm models, and thermodynamic equations along with their parameters; a kinetic plot showing the relationship between percent removal and time (in hours) (Figure S1) (PDF)

■ AUTHOR INFORMATION

Corresponding Author

Dinesh Mohan − *School of Environmental Sciences, Jawaharlal Nehru University, New Delhi 110067, India;* orcid.org/0000-0002-3251-2946; Phone: 0091-11-26704616; Email: dm_1967@hotmail.com

Authors

Jonathan S. Singsit − *School of Environmental Sciences, Jawaharlal Nehru University, New Delhi 110067, India;* orcid.org/0009-0003-0710-8727

Abhishek Kumar Chaubey − *School of Environmental Sciences, Jawaharlal Nehru University, New Delhi 110067, India;* orcid.org/0000-0001-8265-3125

Manvendra Patel − *School of Environmental Sciences, Jawaharlal Nehru University, New Delhi 110067, India;* orcid.org/0000-0002-5801-5526

Complete contact information is available at: https://pubs.acs.org/10.1021/acs.chas.4c00036

Author Contributions

CRediT: **Jonathan S. Singsit** conceptualization, data curation, formal analysis, investigation, methodology, writing - original draft, writing - review & editing; **Abhishek Kumar Chaubey** formal analysis, writing - original draft, writing - review & editing; **Manvendra Patel** formal analysis, writing - original draft, writing - review & editing; **Dinesh Mohan** conceptualization, formal analysis, funding acquisition, investigation, methodology, project administration, resources, supervision, writing - original draft, writing - review & editing.

Notes

The authors declare no competing financial interest.

■ ACKNOWLEDGMENTS

J.S.S. is grateful to University Grants Commission for providing Senior Research Fellowship. D.M. is thankful to PSA, GOI, for financial assistance under the project "Delhi Cluster-Delhi Research Implementation and Innovation (DRIIV)". The authors would like to thank the Board of Research in Nuclear Science (BRNS) (BRNS Sanction No.

56/14/01/2024-BRNS/400), Department of Atomic Energy, Government of India for financial assistance.

REFERENCES

(1) Hignite, C.; Azarnoff, D. L. Drugs and drug metabolites as environmental contaminants: chlorophenoxyisobutyrate and salicylic acid in sewage water effluent. *Life Sci.* **1977**, *20* (2), 337−341.
(2) Patel, M.; Kumar, R.; Kishor, K.; Mlsna, T.; Pittman, C. U., Jr.; Mohan, D. Pharmaceuticals of emerging concern in aquatic systems: chemistry, occurrence, effects, and removal methods. *Chem. Rev.* **2019**, *119* (6), 3510−3673.
(3) Rivera-Utrilla, J.; Sánchez-Polo, M.; Ferro-García, M. Á.; Prados-Joya, G.; Ocampo-Pérez, R. Pharmaceuticals as emerging contaminants and their removal from water. A review. *Chemosphere* **2013**, *93* (7), 1268−1287.
(4) Aus der Beek, T.; Weber, F. A.; Bergmann, A.; Hickmann, S.; Ebert, I.; Hein, A.; Küster, A. Pharmaceuticals in the environment—Global occurrences and perspectives. *Environ. Toxicol. Chem.* **2016**, *35* (4), 823−835.
(5) Ebele, A. J.; Abou-Elwafa Abdallah, M.; Harrad, S. Pharmaceuticals and personal care products (PPCPs) in the freshwater aquatic environment. *Emerging Contam.* **2017**, *3* (1), 1−16.
(6) Muir, D.; Simmons, D.; Wang, X.; Peart, T.; Villella, M.; Miller, J.; Sherry, J. Bioaccumulation of pharmaceuticals and personal care product chemicals in fish exposed to wastewater effluent in an urban wetland. *Sci. Rep.* **2017**, *7* (1), No. 16999.
(7) Cycoń, M.; Mrozik, A.; Piotrowska-Seget, Z. Antibiotics in the Soil Environment-Degradation and Their Impact on Microbial Activity and Diversity. *Front. Microbiol.* **2019**, *10*, 338.
(8) Been, F.; Emke, E.; Matias, J.; Baz-Lomba, J. A.; Boogaerts, T.; Castiglioni, S.; Campos-Manas, M.; Celma, A.; Covaci, A.; de Voogt, P.; Hernandez, F.; Kasprzyk-Hordern, B.; Laak, T. T.; Reid, M.; Salgueiro-Gonzalez, N.; Steenbeek, R.; van Nuijs, A. L. N.; Zuccato, E.; Bijlsma, L. Changes in drug use in European cities during early COVID-19 lockdowns—A snapshot from wastewater analysis. *Environ. Int.* **2021**, *153*, No. 106540.
(9) Reinstadler, V.; Ausweger, V.; Grabher, A. L.; Kreidl, M.; Huber, S.; Grander, J.; Haslacher, S.; Singer, K.; Schlapp-Hackl, M.; Sorg, M.; Erber, H.; Oberacher, H. Monitoring drug consumption in Innsbruck during coronavirus disease 2019 (COVID-19) lockdown by wastewater analysis. *Sci. Total Environ.* **2021**, *757*, No. 144006.
(10) Castiglioni, S.; Bagnati, R.; Fanelli, R.; Pomati, F.; Calamari, D.; Zuccato, E. Removal of pharmaceuticals in sewage treatment plants in Italy. *Environ. Sci. Technol.* **2006**, *40* (1), 357−363.
(11) Onesios, K. M.; Jim, T. Y.; Bouwer, E. J. Biodegradation and removal of pharmaceuticals and personal care products in treatment systems: a review. *Biodegradation* **2009**, *20* (4), 441−466.
(12) Philip, J. M.; Aravind, U. K.; Aravindakumar, C. T. Emerging contaminants in Indian environmental matrices—A review. *Chemosphere* **2018**, *190*, 307−326.
(13) Adams, C.; Wang, Y.; Loftin, K.; Meyer, M. Removal of antibiotics from surface and distilled water in conventional water treatment processes. *J. Environ. Eng.* **2002**, *128* (3), 253−260.
(14) de Andrade, J. R.; Oliveira, M. F.; da Silva, M. G. C.; Vieira, M. G. A. Adsorption of Pharmaceuticals from Water and Wastewater Using Nonconventional Low-Cost Materials: A Review. *Ind. Eng. Chem. Res.* **2018**, *57* (9), 3103−3127.
(15) Ateia, M.; Helbling, D. E.; Dichtel, W. R. Best Practices for Evaluating New Materials as Adsorbents for Water Treatment. *ACS Mater. Lett.* **2020**, *2* (11), 1532−1544.
(16) Westerhoff, P.; Yoon, Y.; Snyder, S.; Wert, E. Fate of endocrine-disruptor, pharmaceutical, and personal care product chemicals during simulated drinking water treatment processes. *Environ. Sci. Technol.* **2005**, *39* (17), 6649−6663.
(17) Homem, V.; Santos, L. Degradation and removal methods of antibiotics from aqueous matrices—a review. *J. Environ. Manage.* **2011**, *92* (10), 2304−2347.
(18) Perreault, F.; Fonseca de Faria, A.; Elimelech, M. Environmental applications of graphene-based nanomaterials. *Chem. Soc. Rev.* **2015**, *44* (16), 5861−96.
(19) Han, Y.; Xu, Z.; Gao, C. Ultrathin Graphene Nanofiltration Membrane for Water Purification. *Adv. Funct. Mater.* **2013**, *23* (29), 3693−3700.
(20) Thompson, K. A.; Shimabuku, K. K.; Kearns, J. P.; Knappe, D. R.; Summers, R. S.; Cook, S. M. Environmental comparison of biochar and activated carbon for tertiary wastewater treatment. *Environ. Sci. Technol.* **2016**, *50* (20), 11253−11262.
(21) Vimal, V.; Patel, M.; Mohan, D. Aqueous carbofuran removal using slow pyrolyzed sugarcane bagasse biochar: equilibrium and fixed-bed studies. *RSC Adv.* **2019**, *9* (45), 26338−26350.
(22) Patel, M.; Kumar, R.; Pittman, C. U., Jr.; Mohan, D. Ciprofloxacin and acetaminophen sorption onto banana peel biochars: Environmental and process parameter influences. *Environ. Res.* **2021**, *201*, No. 111218.
(23) Sarswat, A.; Mohan, D. Sustainable development of coconut shell activated carbon (CSAC) & a magnetic coconut shell activated carbon (MCSAC) for phenol (2-nitrophenol) removal. *RSC Adv.* **2016**, *6* (88), 85390−85410.
(24) Choudhary, V.; Patel, M.; Pittman, C. U., Jr; Mohan, D. Batch and Continuous Fixed-Bed Lead Removal Using Himalayan Pine Needle Biochar: Isotherm and Kinetic Studies. *ACS Omega* **2020**, *5* (27), 16366−16378.
(25) Gao, L.; Goldfarb, J. L. Heterogeneous biochars from agriculture residues and coal fly ash for the removal of heavy metals from coking wastewater. *RSC Adv.* **2019**, *9* (28), 16018−16027.
(26) Kumar, H.; Patel, M.; Mohan, D. Simplified Batch and Fixed-Bed Design System for Efficient and Sustainable Fluoride Removal from Water Using Slow Pyrolyzed Okra Stem and Black Gram Straw Biochars. *ACS Omega* **2019**, *4* (22), 19513−19525.
(27) Sizmur, T.; Fresno, T.; Akgul, G.; Frost, H.; Moreno-Jimenez, E. Biochar modification to enhance sorption of inorganics from water. *Bioresour. Technol.* **2017**, *246*, 34−47.
(28) Grisales-Cifuentes, C. M.; Serna Galvis, E. A.; Porras, J.; Florez, E.; Torres-Palma, R. A.; Acelas, N. Kinetics, isotherms, effect of structure, and computational analysis during the removal of three representative pharmaceuticals from water by adsorption using a biochar obtained from oil palm fiber. *Bioresour. Technol.* **2021**, *326*, No. 124753.
(29) Tran, H. N.; Tomul, F.; Ha, N. T. H.; Nguyen, D. T.; Lima, E. C.; Le, G. T.; Chang, C.-T.; Masindi, V.; Woo, S. H. Innovative spherical biochar for pharmaceutical removal from water: Insight into adsorption mechanism. *J. Hazard. Mater.* **2020**, *394*, No. 122255.
(30) Li, Y.; Taggart, M. A.; McKenzie, C.; Zhang, Z.; Lu, Y.; Pap, S.; Gibb, S. Utilizing low-cost natural waste for the removal of pharmaceuticals from water: Mechanisms, isotherms and kinetics at low concentrations. *J. Cleaner Prod.* **2019**, *227*, 88−97.
(31) Essandoh, M.; Kunwar, B.; Pittman, C. U., Jr.; Mohan, D.; Mlsna, T. Sorptive removal of salicylic acid and ibuprofen from aqueous solutions using pine wood fast pyrolysis biochar. *Chem. Eng. J.* **2015**, *265*, 219−227.
(32) Xu, R. K.; Xiao, S. C.; Yuan, J. H.; Zhao, A. Z. Adsorption of methyl violet from aqueous solutions by the biochars derived from crop residues. *Bioresour. Technol.* **2011**, *102* (22), 10293−8.
(33) Park, J.-H.; Wang, J. J.; Meng, Y.; Wei, Z.; DeLaune, R. D.; Seo, D.-C. Adsorption/desorption behavior of cationic and anionic dyes by biochars prepared at normal and high pyrolysis temperatures. *Colloids Surf., A* **2019**, *572*, 274−282.
(34) Jung, C.; Park, J.; Lim, K. H.; Park, S.; Heo, J.; Her, N.; Oh, J.; Yun, S.; Yoon, Y. Adsorption of selected endocrine disrupting compounds and pharmaceuticals on activated biochars. *J. Hazard. Mater.* **2013**, *263* (Pt 2), 702−10.
(35) Wang, J.; Zhang, M. Adsorption Characteristics and Mechanism of Bisphenol A by Magnetic Biochar. *Int. J. Environ. Res. Public Health* **2020**, *17* (3), 1075.

https://doi.org/10.1021/acs.chas.4c00036
ACS Chem. Health Saf. XXXX, XXX, XXX−XXX

(36) Kumar, A.; Singh, E.; Khapre, A.; Bordoloi, N.; Kumar, S. Sorption of volatile organic compounds on non-activated biochar. *Bioresour. Technol.* **2020**, *297*, No. 122469.
(37) Chen, B.; Chen, Z. Sorption of naphthalene and 1-naphthol by biochars of orange peels with different pyrolytic temperatures. *Chemosphere* **2009**, *76* (1), 127−33.
(38) Xu, X.; Cao, X.; Zhao, L. Comparison of rice husk- and dairy manure-derived biochars for simultaneously removing heavy metals from aqueous solutions: role of mineral components in biochars. *Chemosphere* **2013**, *92* (8), 955−61.
(39) Qian, L.; Zhang, W.; Yan, J.; Han, L.; Gao, W.; Liu, R.; Chen, M. Effective removal of heavy metal by biochar colloids under different pyrolysis temperatures. *Bioresour. Technol.* **2016**, *206*, 217−224.
(40) Navarathna, C. M.; Karunanayake, A. G.; Gunatilake, S. R.; Pittman, C. U., Jr.; Perez, F.; Mohan, D.; Mlsna, T. Removal of Arsenic(III) from water using magnetite precipitated onto Douglas fir biochar. *J. Hazard. Mater.* **2019**, *250*, No. 109429.
(41) Singh, P.; Sarswat, A.; Pittman, C. U., Jr.; Mlsna, T.; Mohan, D. Sustainable Low-Concentration Arsenite [As(III)] Removal in Single and Multicomponent Systems Using Hybrid Iron Oxide-Biochar Nanocomposite Adsorbents-A Mechanistic Study. *ACS Omega* **2020**, *5* (6), 2575−2593.
(42) Salimova, A.; Zuo, J.; Liu, F.; Wang, Y.; Wang, S.; Verichev, K. Ammonia and phosphorus removal from agricultural runoff using cash crop waste-derived biochars. *Front. Environ. Sci. Eng.* **2020**, *14* (3), 1−13.
(43) Su, M. H.; Azwar, E.; Yang, Y.; Sonne, C.; Yek, P. N. Y.; Liew, R. K.; Cheng, C. K.; Show, P. L.; Lam, S. S. Simultaneous removal of toxic ammonia and lettuce cultivation in aquaponic system using microwave pyrolysis biochar. *J. Hazard. Mater.* **2020**, *396*, No. 122610.
(44) Li, J.-h.; Lv, G.-h.; Bai, W.-b.; Liu, Q.; Zhang, Y.-c.; Song, J.-q. Modification and use of biochar from wheat straw (Triticum aestivumL.) for nitrate and phosphate removal from water. *Desalin. Water Treat.* **2014**, *57* (10), 4681−4693.
(45) Divband Hafshejani, L.; Hooshmand, A.; Naseri, A. A.; Mohammadi, A. S.; Abbasi, F.; Bhatnagar, A. Removal of nitrate from aqueous solution by modified sugarcane bagasse biochar. *Ecol. Eng.* **2016**, *95*, 101−111.
(46) Mohan, D.; Sarswat, A.; Ok, Y. S.; Pittman, C. U., Jr. Organic and inorganic contaminants removal from water with biochar, a renewable, low cost and sustainable adsorbent–a critical review. *Bioresour. Technol.* **2014**, *160*, 191−202.
(47) Ahmed, M. B.; Zhou, J. L.; Ngo, H. H.; Guo, W.; Chen, M. Progress in the preparation and application of modified biochar for improved contaminant removal from water and wastewater. *Bioresour. Technol.* **2016**, *214*, 836−851.
(48) Inyang, M.; Dickenson, E. The potential role of biochar in the removal of organic and microbial contaminants from potable and reuse water: A review. *Chemosphere* **2015**, *134*, 232−40.
(49) Oliveira, F. R.; Patel, A. K.; Jaisi, D. P.; Adhikari, S.; Lu, H.; Khanal, S. K. Environmental application of biochar: Current status and perspectives. *Bioresour. Technol.* **2017**, *246*, 110−122.
(50) Chaubey, A. K.; Patel, M.; Pittman, C. U., Jr.; Mohan, D. Acetaminophen and trimethoprim batch and fixed-bed sorption on MgO/Al2O3-modified rice husk biochar. *Colloids Surf., A* **2023**, *677*, No. 132263.
(51) Srivatsav, P.; Bhargav, B. S.; Shanmugasundaram, V.; Arun, J.; Gopinath, K. P.; Bhatnagar, A. Biochar as an Eco-Friendly and Economical Adsorbent for the Removal of Colorants (Dyes) from Aqueous Environment: A Review. *Water* **2020**, *12* (12), 3561.
(52) Sumalinog, D. A. G.; Capareda, S. C.; de Luna, M. D. G. Evaluation of the effectiveness and mechanisms of acetaminophen and methylene blue dye adsorption on activated biochar derived from municipal solid wastes. *J. Environ. Manage.* **2018**, *210*, 255−262.
(53) Shakoor, M. B.; Ali, S.; Rizwan, M.; Abbas, F.; Bibi, I.; Riaz, M.; Khalil, U.; Niazi, N. K.; Rinklebe, J. A review of biochar-based sorbents for separation of heavy metals from water. *Int. J. Phytorem.* **2020**, *22* (2), 111−126.
(54) Nithya, K.; Sathish, A.; Kumar, P. S. Packed bed column optimization and modeling studies for removal of chromium ions using chemically modified *Lantana camara* adsorbent. *J. Water Process Eng.* **2020**, *33*, No. 101069.
(55) Mohan, D.; Pittman, C. U., Jr. Arsenic removal from water/wastewater using adsorbents–A critical review. *J. Hazard. Mater.* **2007**, *142* (1−2), 1−53.
(56) Kumar, R.; Patel, M.; Singh, P.; Bundschuh, J.; Pittman, C. U., Jr.; Trakal, L.; Mohan, D. Emerging technologies for arsenic removal from drinking water in rural and peri-urban areas: Methods, experience from, and options for Latin America. *Sci. Total Environ.* **2019**, *694*, No. 133427.
(57) Mohan, D.; Pittman, C. U., Jr.; Bricka, M.; Smith, F.; Yancey, B.; Mohammad, J.; Steele, P. H.; Alexandre-Franco, M. F.; Gómez-Serrano, V.; Gong, H. Sorption of arsenic, cadmium, and lead by chars produced from fast pyrolysis of wood and bark during bio-oil production. *J. Colloid Interface Sci.* **2007**, *310* (1), 57−73.
(58) Mungi, N. A.; Qureshi, Q.; Jhala, Y. V. Expanding niche and degrading forests: Key to the successful global invasion of *Lantana camara* (sensu lato). *Glob. Ecol. Conserv.* **2020**, *23*, No. e01080.
(59) Sharma, O. P.; Sharma, S.; Pattabhi, V.; Mahato, S. B.; Sharma, P. D. A review of the hepatotoxic plant *Lantana camara*. *Crit. Rev. Toxicol.* **2007**, *37* (4), 313−352.
(60) Ono, M.; Hashimoto, A.; Miyajima, M.; Sakata, A.; Furusawa, C.; Shimode, M.; Tsutsumi, S.; Yasuda, S.; Okawa, M.; Kinjo, J.; Yoshimitsu, H.; Nohara, T. Two new triterpenoids from the leaves and stems of *Lantana camara*. *Nat. Prod Res.* **2021**, *35* (21), 3757−3765.
(61) Kasmara, H.; Melanie; Nurfajri, D. A.; Hermawan, W.; Panatarani, C. The toxicity evaluation of prepared *Lantana camara* nano extract against Spodoptera litura (Lepidoptera: Noctuidae). *AIP Conf. Proc.* **2018**, *1927* (1), No. 030046.
(62) Carstairs, S. D.; Luk, J. Y.; Tomaszewski, C. A.; Cantrell, F. L. Ingestion of *Lantana camara* is not associated with significant effects in children. *Pediatrics* **2010**, *126* (6), e1585−8.
(63) Ghosal, K.; Saha, B.; Gupta Bhattacharya, S. Clinical and immuno-proteomic approach on *Lantana camara* pollen allergy—a major health hazard. *Allergy, Asthma, Clin. Immunol.* **2016**, *12* (1), 33.
(64) Negi, G. C. S.; Sharma, S.; Vishvakarma, S. C.; Samant, S. S.; Maikhuri, R. K.; Prasad, R. C.; Palni, L. M. Ecology and use of *Lantana camara* in India. *Bot. Rev.* **2019**, *85* (2), 109−130.
(65) Gautam, R. K.; Gautam, P. K.; Banerjee, S.; Rawat, V.; Soni, S.; Sharma, S. K.; Chattopadhyaya, M. C. Removal of tartrazine by activated carbon biosorbents of *Lantana camara*: kinetics, equilibrium modeling and spectroscopic analysis. *J. Environ. Chem. Eng.* **2015**, *3* (1), 79−88.
(66) Vo, H. N. P.; Le, G. K.; Nguyen, T. M. H.; Bui, X.-T.; Nguyen, K. H.; Rene, E. R.; Vo, T. D. H.; Cao, N.-D. T.; Mohan, R. Acetaminophen micropollutant: Historical and current occurrences, toxicity, removal strategies and transformation pathways in different environments. *Chemosphere* **2019**, *236*, No. 124391.
(67) Balakrishna, K.; Rath, A.; Praveenkumarreddy, Y.; Guruge, K. S.; Subedi, B. A review of the occurrence of pharmaceuticals and personal care products in Indian water bodies. *Ecotoxicol. Environ. Saf.* **2017**, *137*, 113−120.
(68) UNDP. Sustainable Development Goals, 2024. https://www.undp.org/sustainable-development-goals.
(69) ASTM *ASTM D1762-84-Standard Test Method for Chemical Analysis of Wood Charcoal*; ASTM International: West Conshohocken, PA, 2013.
(70) Lima, D. R.; Hosseini-Bandegharaei, A.; Thue, P. S.; Lima, E. C.; de Albuquerque, Y. R.; dos Reis, G. S.; Umpierres, C. S.; Dias, S. L.; Tran, H. N. Efficient acetaminophen removal from water and hospital effluents treatment by activated carbons derived from Brazil nutshells. *Colloids Surf., A* **2019**, *583*, No. 123966.
(71) Lagergren, S. K. About the theory of so-called adsorption of soluble substances. *Sven. Vetenskapsakad. Handingarl.* **1898**, *24*, 1−39.

https://doi.org/10.1021/acs.chas.4c00036
ACS Chem. Health Saf. XXXX, XXX, XXX−XXX

(72) Ho, Y.; McKay, G. A comparison of chemisorption kinetic models applied to pollutant removal on various sorbents. *Process Saf. Environ. Prot.* **1998**, *76* (4), 332−340.
(73) Foo, K. Y.; Hameed, B. H. Insights into the modeling of adsorption isotherm systems. *Chem. Eng. J.* **2010**, *156* (1), 2−10.
(74) Langmuir, I. The adsorption of gases on plane surfaces of glass, mica and platinum. *J. Am. Chem. Soc.* **1918**, *40* (9), 1361−1403.
(75) Freundlich, H. Over the adsorption in solution. *J. Phys. Chem. A* **1906**, *57*, 1100−1107.
(76) Temkin, M. Kinetics of ammonia synthesis on promoted iron catalysts. *Acta Physiochim. URSS* **1940**, *12*, 327−356.
(77) Redlich, O.; Peterson, D. L. A useful adsorption isotherm. *J. Phys. Chem. A* **1959**, *63* (6), 1024.
(78) Toth, J. State equation of the solid-gas interface layers. *Acta Chim. Hung.* **1971**, *69*, 311−328.
(79) Sips, R. On the structure of a catalyst surface. *J. Chem. Phys.* **1948**, *16* (5), 490−495.
(80) Anastopoulos, I.; Kyzas, G. Z. Are the thermodynamic parameters correctly estimated in liquid-phase adsorption phenomena? *J. Mol. Liq.* **2016**, *218*, 174−185.
(81) Goodhew, P. J.; Humphreys, J.; Beanland, R. The Transmission Electron Microscope. In *Electron Microsopy and Analysis*, 3rd ed.; Goodhew, P. J.; Humphreys, J.; Beanland, R., Eds.; Taylor & Francis, 2001; pp 66−121.
(82) Kim, P.; Johnson, A.; Edmunds, C. W.; Radosevich, M.; Vogt, F.; Rials, T. G.; Labbé, N. Surface functionality and carbon structures in lignocellulosic-derived biochars produced by fast pyrolysis. *Energy Fuels* **2011**, *25* (10), 4693−4703.
(83) Mohan, D.; Abhishek, K.; Sarswat, A.; Patel, M.; Singh, P.; Pittman, C. U., Jr. Biochar production and applications in soil fertility and carbon sequestration—a sustainable solution to crop-residue burning in India. *RSC Adv.* **2018**, *8* (1), 508−520.
(84) Silverstein, R. M.; Webster, F. X.; Kiemle, D. J.; Bryce, D. L. Infrared Spectroscopy. In *Spectrometric Identification of Organic Compounds*; Silverstein, R. M.; Webster, F. X.; Kiemle, D. J.; Bryce, D. L., Eds.; John Wiley & Sons, 2014.
(85) Terzyk, A. P. The influence of activated carbon surface chemical composition on the adsorption of acetaminophen (paracetamol) in vitro: Part II. TG, FTIR, and XPS analysis of carbons and the temperature dependence of adsorption kinetics at the neutral pH. *Colloids Surf., A* **2001**, *177* (1), 23−45.
(86) Bernal, V.; Erto, A.; Giraldo, L.; Moreno-Piraján, J. C. Effect of Solution pH on the Adsorption of Paracetamol on Chemically Modified Activated Carbons. *Molecules* **2017**, *22* (7), 1032.
(87) García-Mateos, F.; Ruiz-Rosas, R.; Marqués, M. D.; Cotoruelo, L. M.; Rodríguez-Mirasol, J.; Cordero, T. Removal of paracetamol on biomass-derived activated carbon: modeling the fixed bed breakthrough curves using batch adsorption experiments. *Chem. Eng. J.* **2015**, *279*, 18−30.
(88) Terzyk, A. P.; Rychlicki, G.; Biniak, S.; Łukaszewicz, J. P. New correlations between the composition of the surface layer of carbon and its physicochemical properties exposed while paracetamol is adsorbed at different temperatures and pH. *J. Colloid Interface Sci.* **2003**, *257* (1), 13−30.
(89) Villaescusa, I.; Fiol, N.; Poch, J.; Bianchi, A.; Bazzicalupi, C. Mechanism of paracetamol removal by vegetable wastes: the contribution of $\pi-\pi$ interactions, hydrogen bonding and hydrophobic effect. *Desalination* **2011**, *270* (1−3), 135−142.
(90) Ahmad, M.; Rajapaksha, A. U.; Lim, J. E.; Zhang, M.; Bolan, N.; Mohan, D.; Vithanage, M.; Lee, S. S.; Ok, Y. S. Biochar as a sorbent for contaminant management in soil and water: a review. *Chemosphere* **2014**, *99*, 19−33.
(91) Mohan, D.; Sharma, R.; Singh, V. K.; Steele, P.; Pittman, C. U., Jr. Fluoride Removal from Water using Bio-Char, a Green Waste, Low-Cost Adsorbent: Equilibrium Uptake and Sorption Dynamics Modeling. *Ind. Eng. Chem. Res.* **2012**, *51* (2), 900−914.
(92) Coimbra, R.; Calisto, V.; Ferreira, C.; Esteves, V.; Otero, M. Removal of pharmaceuticals from municipal wastewater by adsorption onto pyrolyzed pulp mill sludge. *Arab. J. Chem.* **2019**, *12* (8), 3611−3620.
(93) Nourmoradi, H.; Moghadam, K. F.; Jafari, A.; Kamarehie, B. Removal of acetaminophen and ibuprofen from aqueous solutions by activated carbon derived from Quercus Brantii (Oak) acorn as a low-cost biosorbent. *J. Environ. Chem. Eng.* **2018**, *6* (6), 6807−6815.
(94) Mestre, A. S.; Pires, R. A.; Aroso, I.; Fernandes, E. M.; Pinto, M. L.; Reis, R. L.; Andrade, M. A.; Pires, J.; Silva, S. P.; Carvalho, A. P. Activated carbons prepared from industrial pre-treated cork: Sustainable adsorbents for pharmaceutical compounds removal. *Chem. Eng. J.* **2014**, *253*, 408−417.
(95) Nguyen, D. T.; Tran, H. N.; Juang, R.-S.; Dat, N. D.; Tomul, F.; Ivanets, A.; Woo, S. H.; Hosseini-Bandegharaei, A.; Nguyen, V. P.; Chao, H.-P. Adsorption process and mechanism of acetaminophen onto commercial activated carbon. *J. Environ. Chem. Eng.* **2020**, *8* (6), No. 104408.

https://doi.org/10.1021/acs.chas.4c00036
ACS Chem. Health Saf. XXXX, XXX, XXX−XXX